Advances in Water Resources 69 (2014) 65–78

Contents lists available at ScienceDirect

Advances in Water Resources

journal homepage: www.elsevier.com/locate/advwatres

Modeling scale-dependent runoff generation in a small semi-arid watershed accounting for rainfall intensity and water depth

Christoph Langhans [a,*], Gerard Govers [a], Jan Diels [a], Jeffry J. Stone [b], Mark A. Nearing [b]

[a] Department of Earth and Environmental Sciences, KULeuven, Celestijnenlaan 200 E, 3001 Heverlee, Belgium
[b] Southwest Watershed Research Center, USDA-ARS, 2000 E. Allen Rd, 85719 Tucson, AZ, USA

ARTICLE INFO

Article history:
Received 19 October 2012
Received in revised form 31 January 2014
Accepted 24 March 2014
Available online 2 April 2014

Keywords:
Runoff
Runon
Infiltration
Green–Ampt
Modeling
Water depth

ABSTRACT

Observed scale effects of runoff on hillslopes and small watersheds derive from complex interactions of time-varying rainfall rates with runoff, infiltration and macro- and microtopographic structures. A little studied aspect of scale effects is the concept of water depth-dependent infiltration. For semi-arid rangeland it has been demonstrated that mounds underneath shrubs have a high infiltrability and lower lying compacted or stony inter-shrub areas have a lower infiltrability. It is hypothesized that runoff accumulation further downslope leads to increased water depth, inundating high infiltrability areas, which increases the area-averaged infiltration rate. A model was developed that combines the concepts of water depth-dependent infiltration, partial contributing area under variable rainfall intensity, and the Green–Ampt theory for point-scale infiltration. The model was applied to rainfall simulation data and natural rainfall–runoff data from a small sub-watershed (0.4 ha) of the Walnut Gulch Experimental Watershed in the semi-arid US Southwest. Its performance to reproduce observed hydrographs was compared to that of a conventional Green–Ampt model assuming complete inundation sheet flow, with runon infiltration, which is infiltration of runoff onto pervious downstream areas. Parameters were derived from rainfall simulations and from watershed-scale calibration directly from the rainfall–runoff events. The performance of the water depth-dependent model was better than that of the conventional model on the scale of a rainfall simulator plot, but on the scale of a small watershed the performance of both model types was similar. We believe that the proposed model contributes to a less scale-dependent way of modeling runoff and erosion on the hillslope-scale.

1. Introduction

The scale-dependency of runoff and infiltration has been recognized widely. In studies that compare runoff at different scales of a hillslope, scale effects appear as reduced runoff coefficients with increasing scale [1–7]. Models that try to reduce scale-dependency in the calculation of runoff generation have concentrated on various effects. Among the explanations for scale effects, variability and duration of a rainstorm are probably the most uncontroversial ones: even on a perfectly homogeneous surface runoff coefficients can be expected to decrease with slope length (or area) due to the infiltration of runoff water in pervious downstream areas (runon infiltration) during periods of low rainfall intensity and/or after the rainfall event. Stomph et al. [8] have quantified the effect of storm duration and slope length on artificial slopes in the laboratory, finding that shorter rainfall durations and longer slopes produce the largest scale effects. Wainwright and Parsons [9] simulated runoff coefficients with a simple storage model, allowing runon infiltration, which is defined as infiltration of water produced by rainfall excess further upslope [10]. They found that the average rainfall intensity and variability of rainfall strongly influenced runoff coefficients, while the reduction in runoff coefficients with slope length of the simulated hillslope was dependent on slope gradient and the hydraulic roughness coefficient. The effect of spatial variation in infiltration capacity on scale effects is more controversial than the temporal effect. Modeling studies have created randomly distributed hydraulic variables, very often saturated hydraulic conductivities (K_s), with or without spatial correlation, and have computed the sensitivity of runoff production to the coefficient of variance and/or the spatial structure of the variance [10–12]. If runon infiltration is allowed, which means that runoff produced upstream infiltrates if it flows over unsaturated areas, substantial scale effects appear [13–15]. It has been suggested that

* Corresponding author. Current address: Forest and Water Group, Department of Forest and Ecosystem Science, Melbourne School of Land and Environment, University of Melbourne, 221 Bouverie St, 3010 Parkville, Victoria, Australia. Tel.: +61 3 83449304.
E-mail address: christoph.langhans@unimelb.edu.au (C. Langhans).

http://dx.doi.org/10.1016/j.advwatres.2014.03.005
0309-1708/

Notation

A_c	rainfall excess contributing area fraction, –
A_i	flow inundated area fraction, –
b	empirical factor of the inundation-depth relationship, L^{-1}
CON	conventional Green–Ampt model with sheet flow
D	average water depth, L
Δr	unit area net inflow, $L\,T^{-1}$
Δt	time step, T
$\Delta\theta$	difference between initial and saturated volumetric moisture content, $L^3\,L^{-3}$
η_e	effective soil porosity, $L^3\,L^{-3}$
f_e	effective infiltration rate, $L\,T^{-1}$
f_t	potential infiltration rate or infiltrability, $L\,T^{-1}$
F_t	cumulative infiltration at the end of a time step, L
i	rainfall intensity, $L\,T^{-1}$
K_c	average hydraulic conductivity of runoff contributing area, $L\,T^{-1}$
K_e	effective hydraulic conductivity, $L\,T^{-1}$
K_i	average hydraulic conductivity of inundated area, $L\,T^{-1}$
K_s	point-scale saturated hydraulic conductivity, $L\,T^{-1}$
l_p	plot length or modeling unit length, L
LP	large plot
m	exponent of depth-discharge relationship representing turbulence of flow, –
ME	model efficiency, –
μ_f	mean of distribution of infiltrabilities, $L\,T^{-1}$
μ_K	mean of distribution of K_s, $L\,T^{-1}$
n	Manning's roughness coefficient, –
OBJ	objective function, –
P	total precipitation of an event, L
ψ	suction across the wetting front and $\Delta\theta$, L
Q	discharge during time step, $L^3\,T^{-1}$
q_e	unit flow width discharge, plot length–averaged, L^2T^{-1}
Q_e	steady state effective discharge, $L^3\,T^{-1}$
Q_p	peak discharge, $L^3\,T^{-1}$
Q_t	total discharge, L^3
R^2	coefficient of determination, –
r_e	rainfall and runon excess or unit area flow rate, plot-averaged, $L\,T^{-1}$
r_{in}	unit area inflow rate at upper plot boundary, $L\,T^{-1}$
ρ_b	bulk density, $M\,L^{-3}$
r_{out}	unit area outflow rate at lower plot boundary, $L\,T^{-1}$
S	slope gradient, –
SP	small plots
t	time,
θ_i	initial volumetric soil moisture content, before start of rain, $L^3\,L^{-3}$
θ_w	volumetric soil moisture content, $L^3\,L^{-3}$
u	average runoff velocity, $L\,T^{-1}$
WDD	water depth-dependent Green–Ampt model with partial inundation
w_p	plot width, L

heterogeneity in the context of runon infiltration increases scale effects, because the likelihood that runoff flows onto areas of very high infiltration capacity is increased with increasing scale, thereby reducing runoff connectivity [7,16]. However, the effect is dependent on rainfall intensity and duration, the pattern of runoff concentration and typical scale of heterogeneities [17], and it has not been quantified yet.

Runon infiltration is usually modeled as sheet flow entering unsaturated modeling units (cells or pixels), supplying water for infiltration in the same way as rainfall on the whole surface of the modeling unit [e.g. 13]. In such a conceptualization a constant hydraulic conductivity for the whole modeling [13] unit is assumed. Runon infiltration has also been modeled to increase with inundation of a microtopography, albeit without a systematic variation of hydraulic conductivity within the microtopography [10]. However, in environments with a clear microtopographical pattern, the local distribution of hydraulic conductivities is not completely random nor constant, but dependent on the relative elevation within the microtopography. Lyford and Qashu [18] found hydraulic conductivities to be 2.6 times higher under creosote bushes (*Larrea tridentata*) and Palo Verde (*Cercidium microphyllum*), compared to the lower lying inter-shrub area. Similarly, Johnson and Gordon [19] have found 2–2.5 times higher infiltration rates under sagebrush (*Artemisia tridentata*) as compared to the inter-shrub areas. For the Mediterranean semi-arid rangeland environments it has been described how increased infiltration rates occur closer to plants as a consequence of mound build-up and improvement of the physical and chemical soil properties around the plant e.g. [20,21]. Dunne et al. [22] have proposed a model for steady state infiltration that accounts for these systematic patterns. In their model infiltration per unit area increased with increasing runoff water depth towards the foot of a slope. This increase is achieved by inundation of parts of an elevation-dependent distribution of hydraulic conductivities, where higher conductivities are associated with higher elevation of the microtopography. The typical distance between mounded plants may influence runoff thresholds and scale effects [23]. Dunne et al. [22] combined the concept of water depth-dependent infiltration with the concept of partial contributing area for runoff production in order to explain the convex shape of shrub-covered hillslopes in Kenya. However, they did not account for temporal variations in rainfall intensity and/or infiltration capacity. Also in agricultural environments the spatial variation in infiltration capacity shows clear structure, leading to water depth dependent infiltration rates. Bresson and Valentin [24] showed that on tilled fields a sedimentary crust with a low hydraulic conductivity builds up in the micro-valleys while the micro-slopes and ridges are covered by a structural crust with much higher conductivity. Fox et al. [25] have subsequently shown in a laboratory study that this phenomenon can lead to a fourfold increase in average hydraulic conductivity with increasing water depth. Langhans et al. [26–28] have shown that under varying inflow and rainfall intensity rates on small rainfall simulation plots infiltration rates increase as inflow, rainfall intensity, water depth and inundated area increase. They have accounted for these effects in a water-depth dependent infiltration model based on Green–Ampt [27]. Clearly, if runon infiltration is water depth-dependent this may produce scale effects as, generally, water depths can be expected to increase with increasing contributing area. While both temporal variation in rainfall (and infiltration) and the depth-dependency of infiltration may cause scale effects, a modeling framework integrating both effects has not yet been empirically tested on both the rainfall simulation plot-scale and the hillslope or small catchment-scale under natural rainfall conditions.

The model first described in Langhans et al. [27] for a steady state case, integrates temporal, water depth and rainfall intensity effects and enables the exploration of the relative importance of these effects on scale effects. In the present study, behavior and

performance are compared to a similar baseline model without water depth-dependency and with a sheet flow assumption. Data for testing the models were rainfall simulations on plots, and small catchment runoff measurements, constituting two typical scales where we would expect runoff generation rates to decrease from plot- to catchments-scale. We chose to form infiltration expressions with parameters that are effective at the local scale (resolution) of approximately 1 m^2 [29]. The actual resolution of a model unit in a distributed model should be similar to the typical scale length of microtopography to be able to capture the full process of interaction between runoff and microtopography. The typical scale length therefore depends on land use: in agricultural systems, tillage implements determine the width of the microtopography (~0.3 m), while in semi-arid rangeland of the study area shrubs on mounds are organized in intervals of ~1.5 m. An advantage of conceptualizing processes at the local scale is that effective parameters can be readily found by parameterizing the model with rainfall simulation data, because the scale of modeling units and experimental plots are similar and it can be assumed that processes within the experimental plot resemble those of the modeling unit.

In this study we seek to answer the following questions: (1) can we observe scale effects in a data set of rainfall simulations and runoff data from small catchments? (2) Can both watershed-scale infiltration models be successfully calibrated using rainfall simulation data or is calibration from watershed-scale runoff data necessary? (3) Does the incorporation of the water depth-dependency and runon infiltration into a Green–Ampt based model improve performance?

2. Methods

This section describes the site and the rainfall simulation data that were used to parameterize the baseline model and the new model to be tested. Further, this section describes the natural rainfall data that were used to validate the models' results when parameterized with rainfall simulation data and to obtain model parameters by calibration and validation against runoff hydrographs. The parameterization is described in detail in Section 3.4.

2.1. Site description

The Walnut Gulch Experimental Watershed (WGEW) of the United States Department of Agriculture (USDA) is a semi-arid watershed located in Southeast Arizona, southwest United States in the transition zone between the Sonoran and Chihuahua desert (Fig. 1). Runoff occurs mainly in the summer months during and shortly after major convective storms. Storms of lower intensity during winter months rarely produce runoff. Within the WGEW, the Lucky Hills Site is a 0.4 ha sub-watershed (LH-106) with an average slope of 7.6%, and equipped with an H-flume [30]. Fig. 2 is a contour map of the watershed, under-laid with a panchromatic satellite image from 7 July 2010 (Quickbird, 0.6 m resolution). The darker gray areas represent single shrubs or agglomerations of a few shrubs (1–2 m in diameter), within a network of gravely soil or scattered forbs and grasses, mostly with a stony upper soil layer (light grey areas). The soil is classified as very gravely sandy loam without a topsoil [31]. Dominant shrubs species within the watershed include Creosote (*Larrea tridentata*) and Whitethorn (*Acacia constricta*) on mounds of looser, mulched soil with fewer stones (Fig. 3).

2.2. Rainfall simulations and runoff measurements

Rainfall simulations with rainfall intensities between 25 and 216 mm h^{-1} were conducted between 2004 and 2008 during summer months about 100 m south of the outlet of LH-106. Rainfall simulations were conducted with a central oscillating boom rainfall simulator with four nozzles (Veejet 80100) attached at 1.52 m intervals, mounted 3 m above ground, while the plot was protected with a wind shield [32]. Details on the experimental procedure are given in Stone et al. [33]. A dry run at initial soil moisture was followed 45 min later by a wet or very wet run. The experiments chosen as the calibration set were wet and very wet runs from 2007 and 2008 on 6 large plots (LP) of 6.1 by 2 m, with apparent steady state runoff reached after application of at least 5 min of rainfall. These experiments were chosen as the calibration set, because orthogonal photos of the plot during experiments and dye velocity measurements (u, L T^{-1}) existed for them which were required for the parameterization of the model (Table 1). The photos covered the lower 3 m of the runoff plot, and on three transects along the plot width, w_p (L), at lengths of approximately 3.75, 4.5 and 5.25 m from the upper plot border, the width fraction of inundation was measured by visual interpretation. Usually, it could easily be seen which parts were covered by water or not, however, stone pavements protruding through a layer of water occasionally created uncertainty in the visual interpretation. Runoff alternated between more concentrated faster flow around vegetated mounds and broader sheetflow in between. Water often flowed along the lateral plot borders. A trend towards more inundation at the lower end of the plot was not present. Consequently, all three transect measurements were averaged to form a single inundated area fraction (A_i), representative for the plot. Mean flow velocity was computed using the centroid of the electrical resistivity curve measured at the outlet of the plot [34]. Rainfall simulations on large plots from 2004 (four plots), where no photos were taken, and small plots (SP, 0.75 m^2, 3 plots) from 2008, were used as validation (Table 1).

Natural rainfall–runoff events were selected from a continuous period of runoff and rainfall measurements from 2001 to 2010. Rainfall depth was digitally recorded at 1 min increments during periods of rainfall at a gage about 100 m from the outlet of LH-106. The runoff hydrograph was measured also as breakpoint data at the H-Flume (Fig. 2). During this period 718 rainfall events were recorded of which 60 resulted in runoff. All runoff events except for one (23.07.2008) had incident rainfall totals of more than 4.5 mm. Thus, this value was chosen as a minimum threshold for the selection of a dataset of rainfall events to be analyzed. Volumetric soil moisture content at 5 cm depth was measured at a meteorological station 270 m north of LH-106. The maximum value was taken as the effective saturated soil moisture content or effective porosity, η_e (L^3 L^{-3}) = 0.29. To obtain a relevant estimate of initial soil moisture content, θ_i (L^3L^{-3}) a value just before rainfall started was selected for each event. Five rainfall events, of which one was producing runoff (07.07.2001), had no soil moisture measurements. The deletion of these events and the use of the rainfall threshold resulted in a total of 147 rainfall events with 58 producing runoff (Table 1). Selecting rainfall events with a threshold rather than selecting only runoff events reflects the fact that in a rainfall–runoff model rainfall is an independent variable while runoff is the quantity to be predicted.

3. Model descriptions

Two contrasting models for the calculation of infiltration and runoff hydraulics at the local scale of a modeling unit are presented. Both were applied in a distributed model for the calculation of runoff at the small watershed-scale.

3.1. Conventional Green–Ampt model with sheet flow (CON)

The model to which the new proposed model is compared is termed conventional, because it uses equations that are commonly

Fig. 1. Location of the study site in the southwest United States.

used to model runoff on hillslopes. Infiltrability (f_t) at the point-scale, assuming piston-type flow is given by the Green–Ampt Equation [35] [e.g. Eq. 5.4.1 in 36]:

$$f_t = K_s\left(\frac{\psi\Delta\theta}{F_t}+1\right) \tag{1}$$

where K_s is the point-scale hydraulic conductivity ($\mathrm{L\,T^{-1}}$), ψ (L) is the suction across the wetting front and $\Delta\theta$ ($\mathrm{L^3\,L^{-3}}$) is the difference between η_e and θ_i. F_t is the cumulative infiltration at the end of a time step, which is given by Eq. 5.4.2 in Chow et al. [36]:

$$F_t = F_{t-\Delta t} + K_s\Delta t + \psi\Delta\theta\ln\left(\frac{F_t+\psi\Delta\theta}{F_{t-\Delta t}+\psi\Delta\theta}\right) \tag{2}$$

The use of Eqs. (1) and (2) for the application to variable intensity rainstorms has been described by Chu [37]. Under the assumption of zero heterogeneity, point-scale K_s equals the effective hydraulic conductivity K_e ($\mathrm{L\,T^{-1}}$). When the surface becomes saturated at ponding time, infiltration is assumed to occur below a thin continuous water layer covering the whole modeling unit. Equally, runon that enters a modeling unit is effectively distributed over the whole surface area and is added to rainfall to form a common water influx.

For modeling runoff on a hillslope, a roughness coefficient is required for the estimation of flow depth. We chose to use Manning's n, as it can be assumed that flow either becomes turbulent as it concentrates downslope, or it is laminar or intermediate, but much disturbed by roughness elements such as stones or litter. The average flow depth D (L) of the whole modeling unit is calculated as:

$$D = \left(\frac{n}{S^{1/2}}q_e\right)^m \tag{3}$$

where q_e ($\mathrm{L^2\,T^{-1}}$) is the effective or average unit width discharge of a modeling unit, S is the gradient of the water surface, assumed to be equal to the slope gradient, and m is an exponent which is 0.6 for turbulent flow [38].

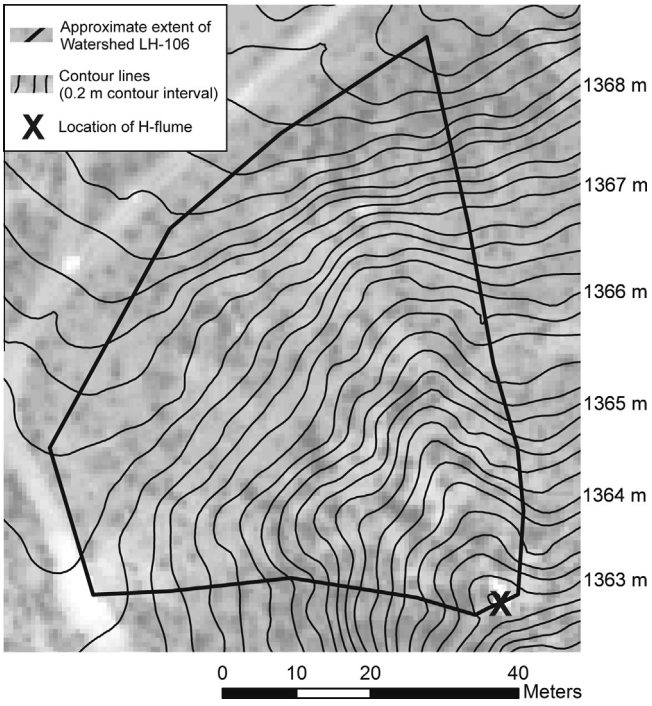

Fig. 2. Contour map of watershed LH-106 in the Lucky Hills Study Area (Fig. 1) with a 0.2 m contour interval. The background is a panchromatic Quickbird image from 7 July 2010. Geographic coordinates of the centre of the catchment are 31°44′32″N, 110°03′14″W.

Fig. 3. Creosote bush on mound and stony inter-shrub area.

At its core, the CON model contains Chu's variable rainfall intensity Green and Ampt infiltration model [37], with the main addition of the possibility of runon infiltration (r_{in}) (Fig. 4)

3.2. Water depth-dependent Green–Ampt model with partial inundation (WDD)

Contrary to the sheetflow assumption, the WDD model acknowledges that there is microtopography. This means that for every level of inundation within the microtopography, there is an average water depth positively correlated to the inundation fraction A_i. The type of this relationship will depend on the microtopography. As a first approximation we used a linear relationship between the inundation fraction and water depth.

$$A_i = bD \tag{4}$$

with b an empirical constant. Eq. (4) does not imply that there is a single channel per modeling unit; it is purely empirical and can contain any amount of micro-channels that can take a tortuous route. These surface and flow characteristics (e.g. flow through protruding stones in this study) are accounted for by Manning's n. As there are inundated and not inundated areas, q_e in Eq. (3) should apply for the inundated area only. The average effective plot unit runoff r_e ($\mathrm{L\,T^{-1}}$) is computed by averaging the inflow r_{in} ($\mathrm{L\,T^{-1}}$) from upslope area and the outflow r_{out} ($\mathrm{L\,T^{-1}}$) from a modeling unit:

$$r_e = (r_{in} + r_{out})/2 \tag{5}$$

Unit width discharge in the WDD model is for width of the inundated area only, so it is defined in relation to re as

$$q_e = l_p r_e A_i^{-1} \tag{6}$$

where l_p (L) is the length of the modeling unit. The depth-discharge relationship can now be adapted for the WDD model, by substituting Eq. (4) into Eq. (6), which was then substituted into Eq. (3):

$$D = \left(\frac{n l_p r_e}{S^{1/2} b}\right)^{\frac{m}{1+m}} \tag{7}$$

Hydraulic conductivities in the WDD model are assumed to have an exponential distribution, an assumption that has been successfully tested elsewhere [33,39,40]:

$$g(K_s) = \frac{1}{\mu_K} \exp\left(-\frac{K_s}{\mu_K}\right) \tag{8}$$

where $g(K_s)$ is the probability distribution of hydraulic conductivities on the scale of the microtopography, within a modeling unit, with μ_K ($\mathrm{L\,T^{-1}}$) their mean, which is assumed constant. We did not assume a random distribution but one that is monotonically increasing with relative elevation of the microtopography, which is in line with field observations (see introduction). This assumption has been made before, but not in conjunction with the exponential distribution [22,25]. Hawkins [39] formalized the partial contributing area approach: at any rainfall intensity (i, $\mathrm{L\,T^{-1}}$), there is always some area where rainfall intensity is limiting infiltration and some area where the soil's infiltration capacity is limiting infiltration, the latter termed runoff contributing area fraction (A_c). In the small-scale context of the microtopography, A_c can be interpreted as the area where water flows erratically, depending on actual raindrop impact towards an inundated area (Fig. 5a). When rainfall starts, A_c is infinitely small, but once soil suction decreases and rainfall intensity increases, a substantial area fraction can contribute to runoff production (Fig. 5a). When water accumulates and concentrates further downstream, or when there is a sudden decrease in rainfall intensity during or at the end of a storm, the accumulated water can inundate an area bigger than A_c (Fig. 5b). In this case runon infiltration will occur on the inundated area. Fig. 5a and b depict a single channel for clarity of the illustration, but the generalized model (Eq. (4)) does not require a specific microtopography form.

In the case of an exponential distribution with a single mean parameter, and when ψ and $\Delta\theta$ are spatially constant, the mean infiltration capacity μ_f ($\mathrm{L\,T^{-1}}$) is proportional to μ_K, just like f_t is proportional to K_s (Eq. (1)) on the point-scale:

$$\mu_f = \mu_K\left(\frac{\psi\Delta\theta}{F_t} + 1\right) \tag{9}$$

Table 1
Basic statistics of the rainfall simulation and rainfall events data set.[a]

	Rainfall simulations[c]			Rainfall events					
	Cal. LP	Val. LP	Val. SP	P (mm)	Q_t[d] (m^3)	Q_e[d] (mm h^{-1})	Q_p[d] (mm h^{-1})	Max. i (mm h^{-1})	θ_i (–)
Number[b]	29 (5)	23 (4)	13 (3)	147	58	58	58	147	147
Mean	125.5	102.7	127.3	11.6	19.0	14.5	25.7	45.0	0.11
STDV	41.1	45.9	52.3	8.5	22.7	15.6	28.3	41.7	0.04
Min	61.5	25.4	46.7	4.6	0.4	0.51	0.69	1.9	0.03
Max	179.5	177.8	216.2	46.4	91.1	55.2	108.6	175.3	0.21

[a] LP: large plots (6 × 2 m), SP: small plots (1.22 × 0.61 m); P: total precipitation of an event; Max i: maximum one minute interval rainfall intensity; θ_i: pre-storm (initial) volumetric water content of soil.
[b] Value in brackets is number of plots.
[c] Statistics refer to applied rainfall intensity (mm h^{-1}).
[d] Q_t: total runoff, Q_e, effective discharge, Q_p: peak discharge; statistics apply to runoff producing events only.

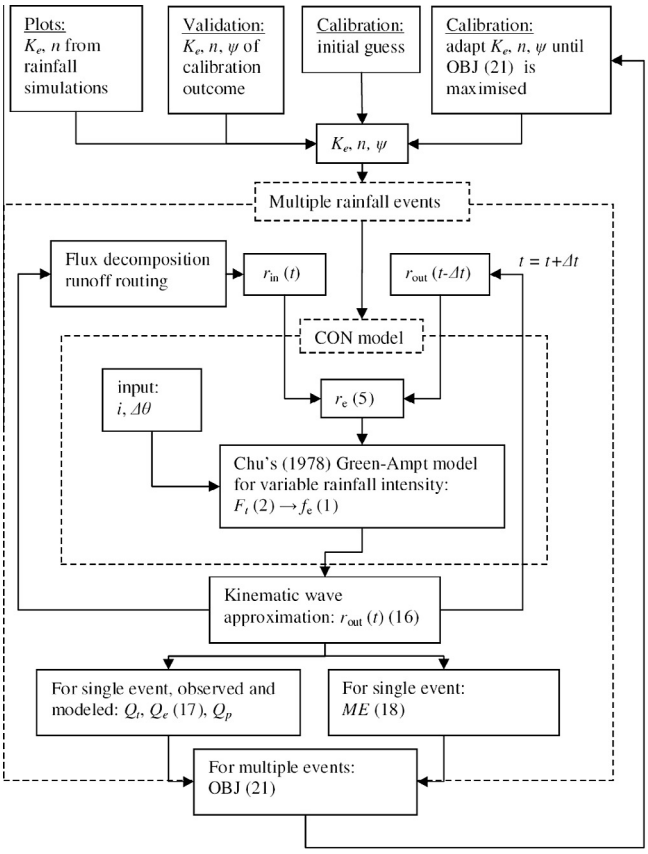

Fig. 4. Flow chart of the CON model and the calibration procedure with multiple rainfall events. Numbers in brackets refer to equations.

Eq. (9) assumes that there is sufficient horizontal redistribution of infiltrated water to form a single infiltration front. It has been shown that an average Green–Ampt infiltration front produced results close to a three-dimensional finite difference solution [41]. F_t, the cumulative infiltration of the time step is not known when it is required in Eq. (9), so the cumulative infiltration of the previous time step $F_{t-\Delta t}$ (with Δt being the time interval) is used as an initial guess (Fig. 6). During subsequent iterations within the time step the value of F_t is updated.

Eq. (9) yields μ_f which is necessary for the calculation of A_c. As A_c is defined as the area fraction where the infiltration capacity is less than the rainfall intensity i, it is obtained by integrating the exponential distribution of infiltration capacities $g(f)$ from 0 to i which yields:

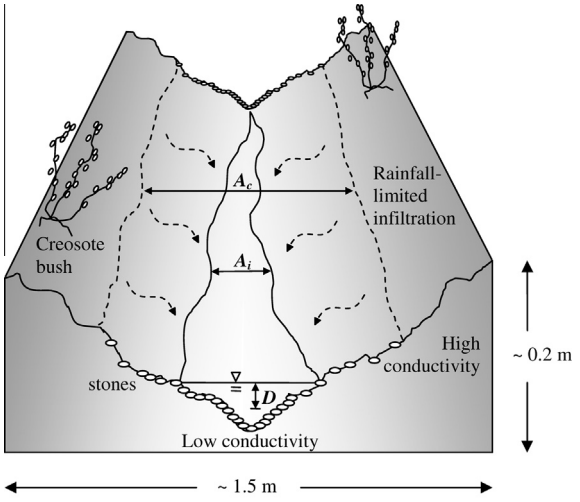

Fig. 5a. Schematic representation of a surface unit during the beginning and middle phase of a rainstorm, when $A_c > A_i$. Rainfall excess erratically flows down the microtopographic slope towards the low conductivity area where inundation starts.

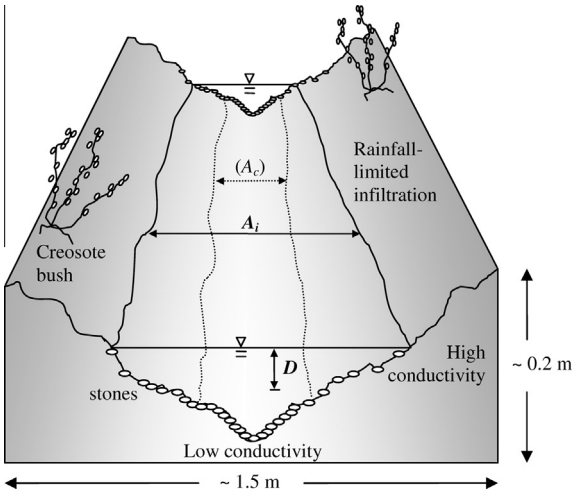

Fig. 5b. Schematic representation of a surface unit during the recession or directly after a rainstorm in an area where runoff concentrates or accumulates, where inundated area (A_i) dominates infiltration.

$$A_c = \int_0^i g(f)df = 1 - \exp\left(-\frac{i}{\mu_f}\right) \tag{10}$$

where $g(f)$ is the same as $g(K_s)$ in Eq. (8), only that μ_K is substituted with μ_f. Like A_c, A_i is also a function of the exponential distribution:

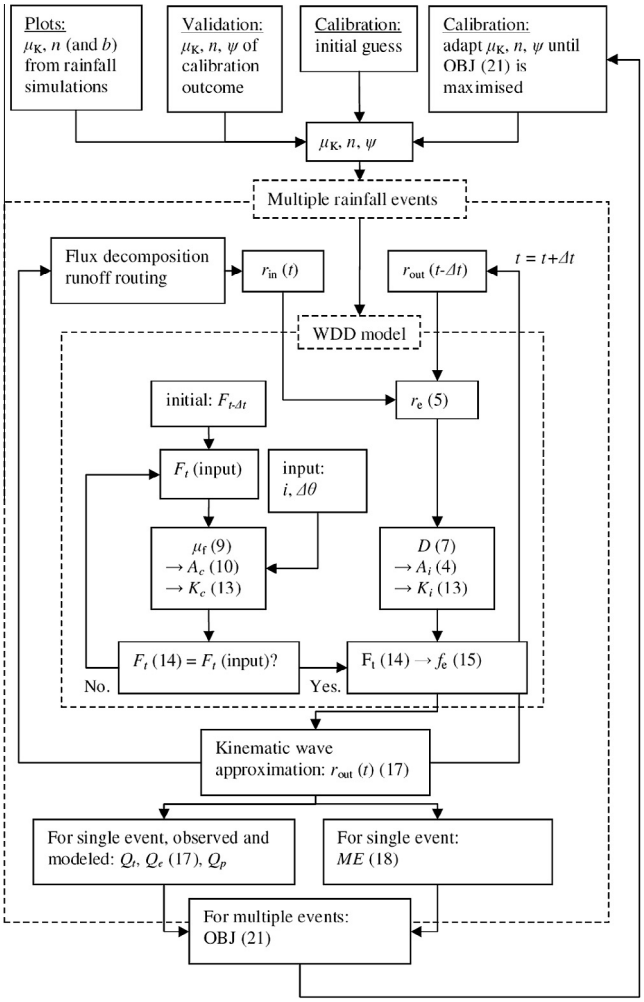

Fig. 6. Flow chart of the WDD model and the calibration procedure with multiple rainfall events. Numbers in brackets refer to equations.

$$A_i = \int_0^{K_s(A_i)} g(K_s)dK_s = 1 - \exp\left(-\frac{K_s(A_i)}{\mu_K}\right) \tag{11}$$

where $K_s(A_i)$ is the hydraulic conductivity at the edge of the water level of inundation. Similarly, $K_s(A_c)$ is the hydraulic conductivity at the edge of the runoff contributing area.

$$K_s(A_{c|i}) = -\ln(1 - A_{c|i})\mu_K \tag{12}$$

where $A_{c|i}$ is either A_c or A_i. The average hydraulic conductivity of the runoff contributing area K_c and the average hydraulic conductivity of the inundated are K_i are obtained by integrating hydraulic conductivities from the exponential distribution $g(K_s)$ from 0 to $K_s(A_{c|i})$, which yields:

$$K_{c|i} = \int_0^{K_s(A_{c|i})} K_s g(K_s)dK_s = \mu_K - (1 - A_{c|i})(\mu_K + K_s(A_{c|i})) \tag{13}$$

where $K_{c|i}$ is either K_c or K_i. F_t can now be calculated as:

$$F_t = F_{t-\Delta t} + i\Delta t(1 - A_{c|i}) + A_{c|i}\left(K_{c|i}\Delta t + \psi\Delta\theta \ln\left(\frac{F_t + \psi\Delta\theta}{F_{t-\Delta t} + \psi\Delta\theta}\right)\right) \tag{14}$$

with $A_{c|i} = A_i$ and $K_{c|i} = K_i$ if $A_i > A_c$ (case Fig. 5b), and else $A_{c|i} = A_c$ and $K_{c|i} = K_c$ (case Fig. 5a). Eq. (14) is derived from Eq. (2), splitting the cumulative infiltration into a part where rainfall infiltrates directly (the second term) and a part where infiltration during a time step under A_i or A_c is limited by the soil (the third term). The resulting value of F_t is still an approximation and the calculation of Eqs. (9)–(14) are repeated until F_t used in Eq. (9) differs from the outcome in Equation 15 by less than a very small threshold value. The effective infiltration rate f_e ($L\,T^{-1}$) of the modeling unit is now given by:

$$f_e = i(1 - A_{c|i}) + K_{c|i}\left(\frac{\psi\Delta\theta}{F_t} + 1\right)A_{c|i}. \tag{15}$$

The first term is infiltration equal to rainfall intensity on the non-inundated and no runoff producing part of the soil and the second term describes infiltration according to the Green–Ampt equation on the remaining inundated or runoff producing area.

3.3. 2D distributed model

Both infiltration models are implemented in MCST [47], a spatially distributed runoff–erosion model that originally used a modified curve number approach. The model routes runoff using the kinematic wave equation in conjunction with a flux decomposition algorithm [43,48].

A digital elevation model of the watershed with a 1 m horizontal resolution from a RTK GPS survey with 426 elevation points was used [42]. Infiltration and runoff calculation was changed so that runon infiltration could be accounted for in each grid cell and at each time step. Following the logic of the linear scheme of the kinematic wave algorithm, r_e in Eq. (5) was calculated with r_{in} as inflow into a modeling unit during the present time step and r_{out} as the outflow calculated on the same modeling unit during the previous time step. In the CON model the estimate of r_e was added to the rainfall intensity to calculate the amount of water which was available for infiltration on the whole surface of the modeling unit in accordance with the sheet flow assumption. In the WDD model, r_e was used to calculate D (Eq. (7)) and A_i (Eq. (4)) and then infiltration as described above. For a given set of parameter values controlling infiltration the WDD model will always predict lower runon infiltration for the same runon amount, unless there is full inundation. Once infiltration is calculated in both models, an estimate for the net lateral inflow into a modeling unit during a time step, Δr ($L\,T^{-1}$), is obtained, which can become negative during runon infiltration, and is given by the difference between rainfall intensity and infiltration. It relates to the kinematic wave equation as:

$$\frac{\partial(r_{out}l_p)}{\partial l_p} + \frac{\partial D}{\partial t} = \Delta r = i - f_e \tag{16}$$

Eq. (17) was solved using a discrete non-linear scheme [36]. So for each time step and modeling unit, runoff, infiltration, water depth, and in the case of the WDD model, inundated area fraction are estimated. For a single rainfall event, three main output quantities were calculated that could be compared to measured quantities: the total discharge, Q_t (L^3), which is the sum of discharge of all time steps at the modeling unit (cell) that represents the outlet of the watershed. The steady state effective discharge, Q_e ($L^3\,T^{-1}$), is a quantity that is used in erosion modeling, also in the MCST model, and is given by [43]:

$$Q_e = \left(\frac{\sum_{t=t_1}^{t_n} Q^{1.4}}{\sum_{t=t_1}^{t_n} Q}\right)^{2.5} \tag{17}$$

where Q ($L^3\,T^{-1}$) is the discharge during one time step t, with t_1 the first and t_n the last time step of an event. The third quantity is peak discharge, Q_p, ($L^3\,T^{-1}$). All three quantities can be modeled and also derived from observational hydrographs, measured at the H-flume at the watershed outlet.

3.4. Model parameterization and evaluation

In accordance with the second objective, the model was parameterized using the calibration set of rainfall simulations to find values for K_e and μ_K for the CON and the WDD model, respectively, and values of Manning's n and the parameter b, the latter for the WDD model. Secondly, K_e, μ_K, ψ and n were calibrated for natural rainfall–runoff events by optimizing an objective function consisting of the Nash–Sutcliffe model efficiency (ME) and the coefficient of determination (R^2) of predictions of Q_t, Q_e and Q_p, where R^2 was defined as:

$$R^2 = \mathrm{ME} = 1 - \frac{\sum_{i=1}^{n}(X_{observed} - X_{predicted})^2}{\sum_{i=1}^{n}(X_{observed} - X_{mean})^2} \quad (18)$$

where X is the quantity of interest. When Eq. (19) is used to calculate ME, X is the instantaneous runoff rate during a time step. All parameters were assumed to be constant within the catchment.

3.4.1. Parameterization using rainfall simulations

An estimate of average plot width flow depth on the rainfall simulation plots (assuming sheet flow) was obtained for the CON model using measured average velocities:

$$D = \frac{r_e l_p}{u} \quad (19)$$

where r_e was calculated from Eq. (5) with measured r_{out} and zero r_{in}. This allowed to find a value for Manning's n that minimized the square of the residuals between predicted and measured D, using observed D, r_e and S data (least squares method) (Eq. (3)).

For the WDD model, D is defined for the inundated area only, so Eq. (20) becomes:

$$D = \frac{r_e l_p}{u A_i} \quad (20)$$

A_i values were measured as described in Section 2.2. D in Eq. (21) was substituted with A_i/b (Eq. (4)) and then b was optimized with the least squares method for predicted and measured r_{out}. Similarly to the CON model, Manning's n could now be found with the least squares method (Eq. (7)).

As K_e was assumed to approximately equal measured final infiltration rates during the (wet run) rainfall experiments, for the CON model an estimate of average K_e is simply derived by averaging final infiltration rates of the calibration dataset. For the WDD model, μ_K was optimized as described and depicted in Fig. 9, dashed area, in Langhans et al. [27] for the steady state case of the rainfall simulation plots.

3.4.2. Calibration on multiple rainfall events

The dataset of 147 rainfall events (Table 1) was randomly split into a calibration set of 74 events and a validation set of 73 events. In accordance with objective 3, optimized parameter sets were found for the CON and the WDD model from the calibration set to assess the water depth-dependency effect, and for both models parameter sets were found that assess the effect of runon infiltration. For the CON model this was done by forcing r_{in} to be zero during infiltration calculation, and for WDD this was done by forcing A_i to be zero during infiltration calculation. The objective function (OBJ) was defined as:

$$\mathrm{OBJ} = \frac{\mathrm{ME} + \frac{R^2(Q_t)+R^2(Q_e)+R^2(Q_p)}{3}}{2} \quad (21)$$

In words, during optimization, the mean R^2 of the predictions of total, effective, and peak discharge was given equal weight as ME. For CON, ψ, K_e and Manning's n, and for WDD ψ, μ_K and Manning's n were simultaneously optimized using the following simple set search method. Starting values within realistic bounds were chosen, and parameter combinations were added that were half the starting value's step in each direction of the parameter space (with three calibration parameters, this results in a 3D grid, when visualized). For each parameter combination in the set, OBJ was calculated, and the combination with the largest value was chosen. This combination was used as a new starting point for another set search, but with half a step size compared to the previous iteration. The number of iteration was limited by computation time but usually exceeded 4. It was ensured that OBJ were indeed maximized within the search space by plotting OBJ. The accuracy was between 1 and 5 mm for ψ, 0.5 mm/h for K_e and μ_K, and 0.002 for Manning's n.

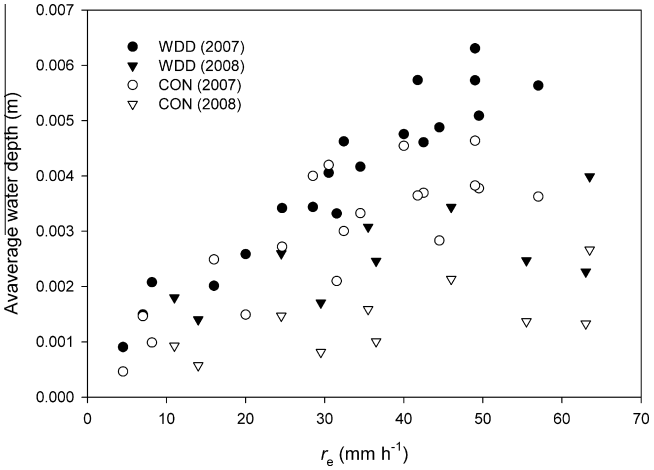

Fig. 7. Relationship between average water depth and effective discharge for 2007 and 2008 on the rainfall simulation plots. In the CON model water depth is calculated for the whole plot width, while in the WDD model it is calculated for the inundated area only.

4. Results

4.1. Rainfall simulations

Water depth of the inundated area show has a clear positive relationship with effective discharge (WDD, Fig. 7), with little scatter for the year 2007. Also, 2007 water depth values are much higher than values of plots from 2008, while the latter level off at 0.002–0.003 m at high flow rates. The D–r_e relationship under the sheet flow assumption (CON, Fig. 7) shows more scatter and lower depth estimates at higher flow rates, as can be expected, because flow is spread over the whole plot. The relationship of A_i–r_e (not shown) gives the same picture as WDD depths in Fig. 7, because A_i and D are related only with the proportionality parameter b. The range of measured inundation fractions was 0.1–0.7. Values for Manning's n were 0.26 and 0.57 for CON and WDD, respectively.

Final infiltration rates (K_e) in the years 2007 and 2008 were much higher than they were in 2004, which were used as validation data (Fig. 8). K_e on the small plots in 2008 were more closely in the range of the infiltration values on the long plots. Moreover, K_e showed a stronger dependency on rainfall intensity in 2007 and 2008 than in 2004. Average K_e, used in the CON model is a constant at 57.2 mm h^{-1}, while μ_K (WDD) was optimized at 62.4 mm h^{-1} (Table 2). In order to clarify the models' behavior on the rainfall simulation plot-scale, final infiltration rates were modeled for a range of rainfall intensities for the 6 m plot, with an average slope of 0.14. The WDD model predicts that the inundation effect (infiltration in area where A_i exceeds A_c) is strongest around the mean of

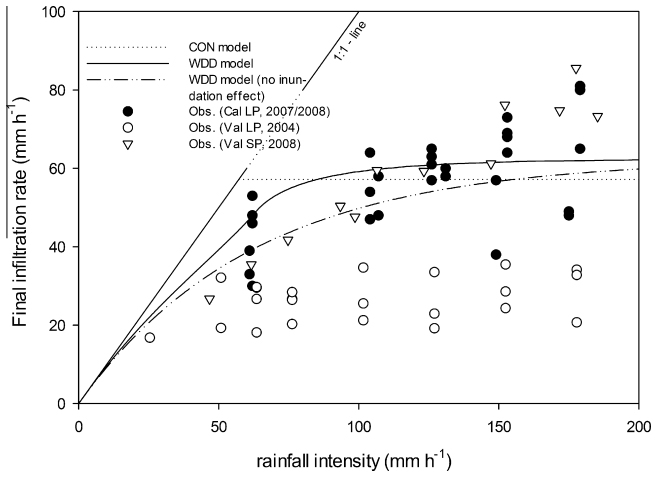

Fig. 8. Relationship between observed final infiltration rates and rainfall intensity under simulated rainfall. Lines are modeled averages of the CON model (dotted), the WDD model without runon infiltration (dashed), and the WDD model with runon infiltration (solid).

the distribution on the 6 m plot (solid line departing from dash-dotted line in Fig. 8). For the 1 m plots the curve for the average predicted K_e lies much closer to the curve of the dashed line, because, relatively, less runon infiltration occurs on a shorter slope (line not shown). Calculated complete inundation at higher rainfall intensities is a bias produced by the assumption of a linear relationship between average water depth and inundation. Actually, there are always some parts of the plot, such as mounds under creosote bushes that remain un-inundated.

Final infiltration rates on long plots were much lower during 2004 (validation), and both models had negative R^2. For the small plots (2008), however, the WDD model yielded better predictions (R^2 = 0.86) compared to the CON model (R^2 = 0.10).

4.2. Calibration with rainfall–runoff events

Parameter values derived from rainfall simulations were used to model runoff hydrographs of all 147 rainfall events. With hardly any runoff predicted, both models performed poorly, with negative R^2 (Eq. (19)) (results not shown). Calibration on multiple events at field-scale yielded much lower optimized values for K_e and μ_K, both for model runs with and without runon infiltration (Table 2). Also, Manning's n values were much smaller than the rainfall experiments suggested. Optimized ψ values were much higher for the WDD than the CON model. The optimization process during calibration yielded clearly defined maxima and smooth contours for OBJ in the parameter space for both models (Fig. 9).

For the calibration set 37% of rainfall–runoff events for both, CON and WDD, had ME values above 0.75 (Table 3). The WDD model however had a higher proportion of events above 0.75 for the validation set. Coefficients of determination for Q_t, Q_p, and Q_e were good for all models and OBJ values were slightly higher for the WDD model than the CON model. The CON model performed slightly better in validation with runon infiltration than without runon infiltration. Comparing observed vs. predicted Q_t revealed that CON had too many events predicting no runoff where there was runoff observed, and, conversely, the WDD model always predicted some runoff, leading to slight overestimation at low runoff rates (figure not shown).

4.3. Model behavior

Model behavior was further studied by comparing predictions of hydrographs with actually observed hydrographs, and by exploring the effects of water depth-dependency and runon infiltration through calculating infiltration under a steady rain (Fig. 10). For a 40 mm h^{-1} synthetic rainstorm of 30 min, the average watershed-scale infiltration rate for the CON model was equal to rainfall intensity for the first 10 min, after which it dropped to below 23 mm h^{-1} at 30 min. When allowing runon infiltration,

Table 2
Optimized parameter values calibrated for the watershed scale from runoff hydrographs for both models (CON and WDD), with and without runon infiltration, and parameters optimized for steady state rainfall simulation plot infiltration ('plot').

	CON		WDD		Plot	
	With runon infiltration	Without runon infiltration	With runon infiltration	Without runon infiltration	CON	WDD
Ψ (mm)	31	22	139	175	–	–
μK (mm h^{-1})	–	–	16.5	14.5	–	62.4
K_e (mm h^{-1})	8	14	–	–	57.2	–
Manning's n	0.085	0.05	0.028	0.026	0.27	0.57

Table 3
Fraction of modeled events with a Nash–Sutcliffe model efficiency (ME) in a given class, coefficients of determination (R^2) for measured vs. modeled Q_t, Q_e and Q_p for all rainfall events, and objective measure (OBJ, Eq. (21)). Parameters were optimized to maximize OBJ, given the CAL dataset and validated with the VAL dataset (Table 1). Both models were calibrated with and without runon infiltration.

		CON without runon		CON without runon		WDD with runon		WDD without runon	
		CAL	VAL	CAL	VAL	CAL	VAL	CAL	VAL
ME	>0.75	0.37	0.11	0.37	0.21	0.37	0.32	0.37	0.29
	0.75 > x > 0.5	0.1	0.14	0.07	0.11	0.23	0.15	0.23	0.18
	0.5 > x > 0	0.13	0.21	0.16	0.18	0.07	0.07	0.07	0.07
	<0	0.4	0.54	0.4	0.5	0.33	0.46	0.33	0.46
R^2	Q_t	0.82	0.62	0.88	0.76	0.94	0.86	0.94	0.85
	Q_p	0.91	0.67	0.94	0.69	0.89	0.72	0.89	0.72
	Q_e	0.93	0.78	0.94	0.74	0.93	0.79	0.93	0.79
OBJ		0.66	0.48	0.66	0.55	0.70	0.59	0.70	0.59

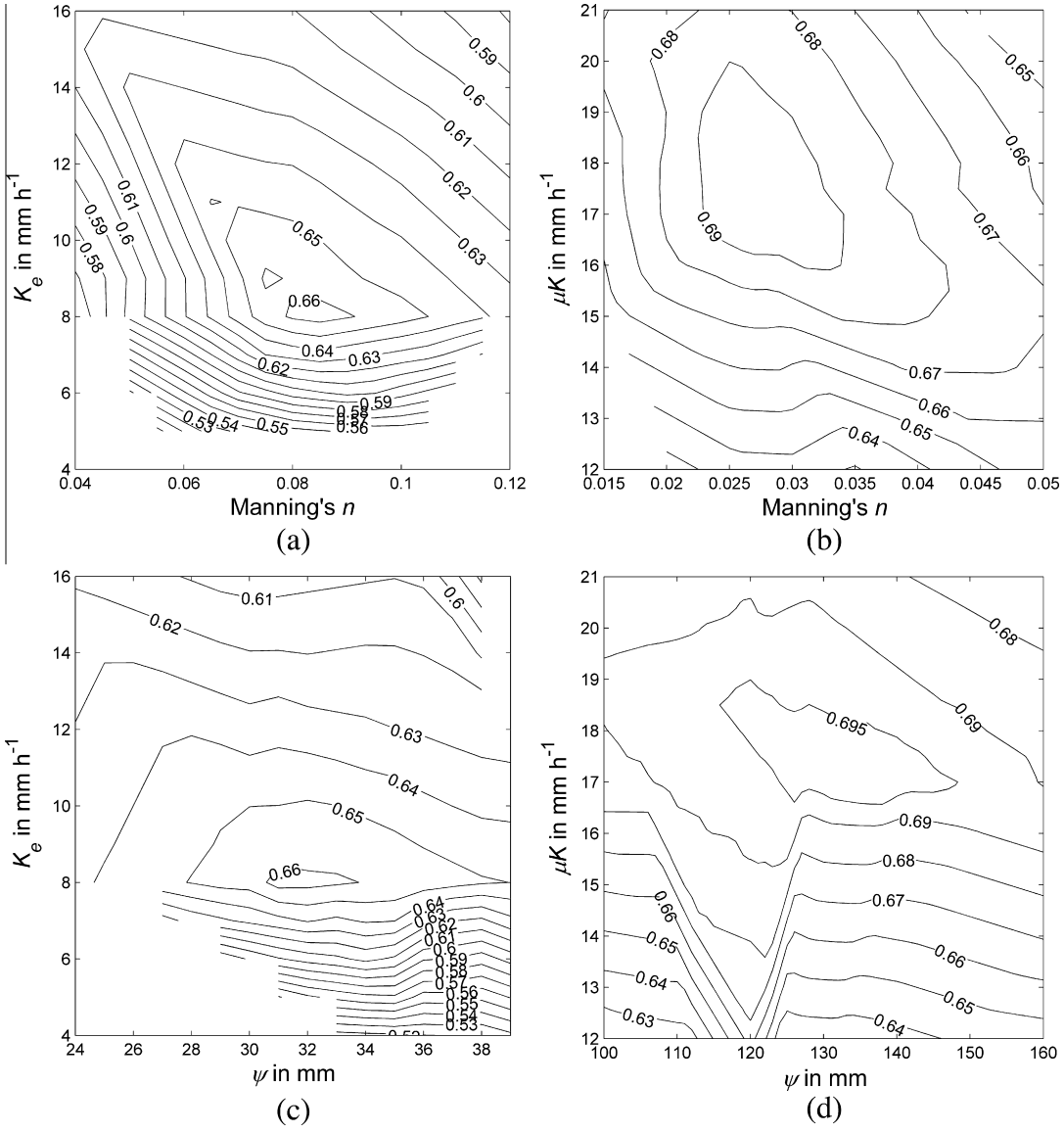

Fig. 9. Contour plots of the OBJ value in the parameter space: (a) Manning's n vs. K_e for CON, (b) and (c) are reversed. (b: Manning's n vs. μK, c: ψ vs. K_e), (d) ψ vs. μK for WDD.

substantial runon infiltration occurred with the CON model between 30 and 40 min. For the WDD model infiltration rates dropped immediately after onset of rainfall to below 20 mm h^{-1} at 30 min. When accounting for runon infiltration, infiltration rates of WDD are only less than 0.5 mm h^{-1} larger from minute 8 onwards compared to WDD without runon infiltration, and after 30 min runon infiltration drops immediately to 1.5 mm h^{-1} only. Water depth-dependent infiltration under such a scenario is thus negligible, whereas runon infiltration in the CON model is important.

For qualitative analysis of the goodness of hydrograph prediction with the watershed-scale calibration parameters, six events were chosen and displayed: The 90th, 50th, and 10th percentile event, based on descending ranking of ME, both for CON and WDD, with runon (Fig. 11).

For the 90th percentile events, the timing of the peak and peak discharge were better predicted for CON than WDD (Fig. 11a and b). For the 50th percentile events, peak discharge was predicted better with the WDD model (Fig. 11c and d), but timing was either worse (Fig. 11c) or better (Fig. 10d) than

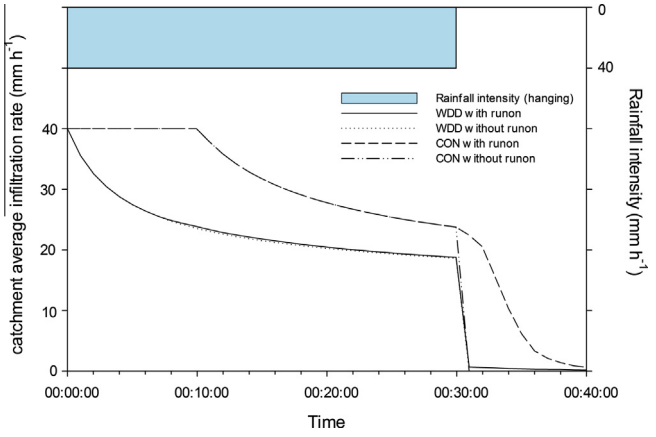

Fig. 10. Catchment average infiltration rate vs. time for a synthetic 30 min storm with 40 mm h^{-1} rainfall intensity. Infiltration rates of the WDD model with runon infiltration (solid) and without runon infiltration (dotted), and of the CON model with runon infiltration (dashed) and without runon infiltration (dash-dotted) are shown.

CON. For the 10th percentile, WDD had a stronger over estimation of peak discharge than CON (Fig. 11e and f), and timing was not apparently wrong. Regarding the form of the hydrographs, WDD generally has a steeper rise than CON, and follows rainfall intensity more closely. CON hydrographs are usually slightly better timed. Generally, however, over- or under-predictions of total or peak discharge not systematic, except, perhaps a tendency of WDD to over-predict during small events and under-predict during larger events.

5. Discussion

5.1. The role of rainfall simulations in watershed-scale models

Rainfall simulation is a widely used tool to infer local scale infiltration parameters and characteristics. Orthogonal photos are an excellent way to gather additional information about runoff characteristics, like inundation and flow paths relative to microtopography. The method of deriving inundated area fractions is

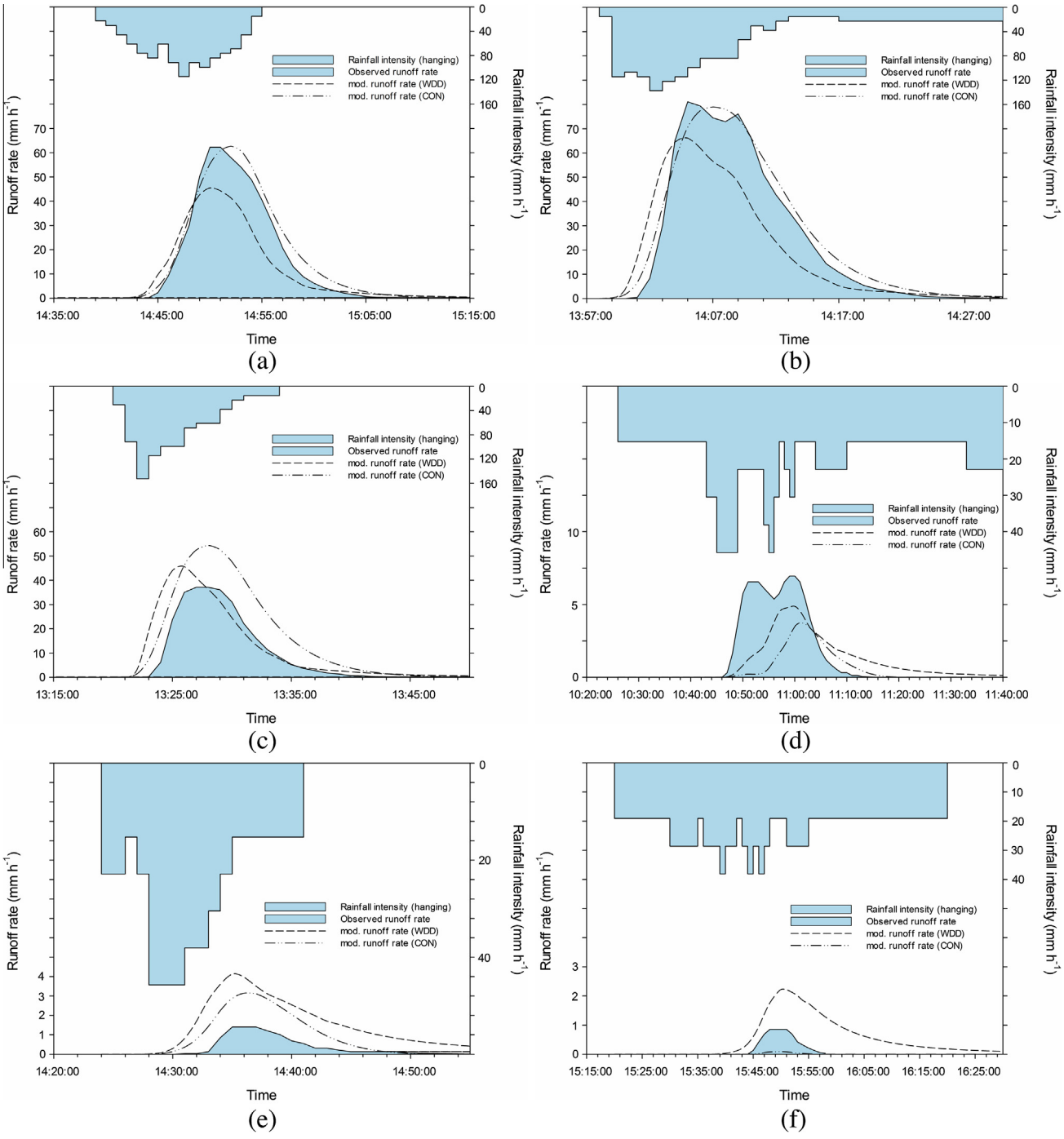

Fig. 11. Modeled and observed hydrographs of the 90th (a: CON, b: WDD) 50th (c: CON, d: WDD) and 10th (e: CON, f: WDD) percentile events based on descending ranking of ME for the CON and the WDD models. Observed hydrographs are solid-shaded and modeled hydrographs are dashed (WDD) and dash-dotted (CON). Rainfall intensity is displayed as stepped, solid line with an inverted scale on the right.

particularly useful, because they can be directly linked to depth-discharge relationships (Eqs. (4) and (7)). Despite some inter year variability, calculated depths and effective runoff show a clear relationship (Fig. 7). The range of average depth values (<1–7 mm) lies within the range that Abrahams and Parsons [44] measured at a similar site on the WGEW. Direct, high precision measurements of runoff water depth [45] or combined inundation and microtopographical measurements for the calculation of water depth are surely superior to inference from flow velocity. However, even in the absence of more direct depth measurements, taking inundation into account will yield more realistic average water depths than the sheet flow assumption, because flow on a small scale hardly ever covers the whole surface where microtopography is present [46].

Values of Manning's n calibrated from the natural rainfall–runoff events were lower with a factor of 3 for the CON model and 19 for the WDD model compared to values derived from rainfall simulations, and K_e and μ_K were four to five times lower (Table 2). There are several possible explanations for this discrepancy, but none taken on its own is sufficient. Regarding hydraulic roughness, it was observed from the orthogonal photos that plot borders impeded flow around mounds of creosote bushes. This must have led to more inundation and higher water depths than would occur in a natural setting without plot borders, where flow can follow unimpeded low lying channels between mounds. This means that on the plot average flow velocities were lower and Manning's n higher than in a natural setting. Certainly, the plot borders increase ponding and with it final infiltration rates during rainfall simulations, but it is unlikely that the effect can explain a four to five -fold difference. Runoff experiments in 2004 still had roughly 2.5 times higher final infiltration rates than the calibrated values. Higher infiltration rates are a common observation for rotating or oscillating boom rainfall simulators. Risse et al. [47] and Nearing et al. [48] have reported 2–4 times higher K_e for rainfall simulations than calibrated values from runoff measurements on larger scale for humid environments. Burns [49] reported for the WGEW site 3–6 times higher rainfall simulation derived K_e than were calibrated for the small watershed-scale. The source of this discrepancy has not been reported. Beside the plot border effect, we can briefly point out three areas of explanation that can contribute to the difference. First, the oscillating boom rainfall simulator has intermittent, very high rainfall intensities with no rainfall in between. According to the partial area response concept, during the high rainfall intensity bursts, high infiltration rates can be achieved, while only time-averaged rainfall intensity is reported that would lead to a much lower infiltration rate. Secondly, there could be a bias during rainfall simulation site selection towards higher infiltration 'interrill' areas. Finally, during rainfall simulations air can escape laterally, which is not possible under natural rainfall which covers the whole area.

As infiltration was higher on the small rainfall simulation-scale, scale effects were the inverse of what one would expect from runon-infiltration theory. But given the above-mentioned differences between rainfall simulations and watershed-scale natural rainfall runoff measurements that can possibly affect infiltration rates, it can be concluded that the two types are incomparable for the purpose of scale enquiry, at least under the studied conditions and environment. This implies that rainfall simulations cannot simply be used for the parameterization of any of the two predictive models, which is confirmed by their bad performance when parameterized with rainfall simulation data in this study. Nevertheless, rainfall simulations can be a valuable tool to study depth-discharge relationships, and relative differences of infiltration between sites and environments, or indeed to study any sub-processes of infiltration in more detail.

5.2. Importance of water depth-dependency and runon infiltration

Both models can predict hydrographs satisfactorily when calibrated on the watershed-scale (Table 3). The water depth-dependent model (WDD) performs slightly better than the conventional sheet flow model (CON), but this improvement is not related to the inundation effect, as the effect is probably very small when parameterized with a relatively low Manning's n of 0.028 (Fig. 10). Possibly, the main improvement above CON stems from the responsiveness of runoff to rainfall, because WDD contains a distribution of hydraulic conductivities, where low conductivities already respond with runoff production at low rainfall intensities. For the CON model, the inclusion of runon infiltration improves performance slightly (Table 3). This supports the theoretical importance of runon infiltration pointed out already by other researchers [10,13].

There are three model structural reasons and one physical reason why water depth-dependent infiltration and runon infiltration does not show up to be important in the WDD model in this study. First, Langhans et al. [27] have shown in a synthetic study that scale effects due to the water depth effect can be significant, but they used a relatively high hydraulic roughness value derived from rainfall simulations. In this study, hydraulic roughness is relatively low, and significant water depths that cause water depth-dependent infiltration do not build up. The physical reason, related to this, is that the macrotopography in the study catchment is very rugged so that runoff concentrates very quickly in channels and the effective hillslope lengths are very short; water depth cannot build up sufficiently on such short slopes. The second model structural reason is that the exponential distribution assumed here (Eq. (8)) is such that only at high inundation levels significant infiltration can occur. If a different distribution had been chosen the water depth effect could have been more pronounced, such as the log-normal distribution which had been suggested before for variation of K_{sat} at larger scales [50–52]. But the analytical solution of the concept described here (i.e. Eqs. (8)–(16)) is not applicable to all distributions and it would require a more stochastic, quasi-empirical approach to formulate the model with empirical or more complex distributions. The third model structural reason is that the assumption that hydraulic conductivities are strictly monotonously increasing within the microtopography is probably too strict. Some randomness within a modeling cell, and between would increase the chance of runon infiltration. A full study of various model structure-related effects, such as the choice of distribution, cell resolution, or randomness would be desirable but is beyond the scope of this study, as most would require a significant reformulation of the model. Consequently, and despite strong theoretical justification of the water depth-dependent infiltration process as pointed out in the introduction, the evidence for the water depth effect remains inconclusive from this study. Future research into the water depth effect and runon infiltration should therefore occur under more controlled field conditions that are tailored to quantify locations and flow pathways during infiltration. Only then it is reasonable to include these effects into models for prediction purpose.

6. Conclusions

The pattern of high infiltrability areas on mounds underneath shrubs and lower lying low infiltrability areas in the inter-shrub area has previously been demonstrated for semi-arid rangeland. Within the concept of water depth-dependent infiltration, runoff accumulation further downslope leads to increased water depth inundating high infiltrability areas, which increases the area

average infiltration rate, one of many explanations for observed scale effects in runoff and erosion. A model was developed that combines the concepts of water depth-dependent infiltration, partial contributing area under variable rainfall intensity, and the Green–Ampt theory for point-scale infiltration. The model was applied to rainfall simulation data and natural rainfall–runoff data from a small semiarid watershed (0.4 ha) in the US Southwest. The model performance was compared to the performance of a conventional Green–Ampt model with the sheet flow assumption. Both models were parameterized with rainfall simulation data, and by calibration from watershed-scale runoff measurements. Parameters of hydraulic roughness and conductivity were larger by a high multiple for the former compared to the latter. This implies that scale effects were the inverse of the expectation, and rainfall simulation plot-scale data could not be used to successfully predict hydrographs. Calibrated models both had good performance, with the water depth-dependent model being slightly better. While runon infiltration was important in improving performance of the sheet flow assumption model, water depth effect was negligible in the new model. This was explained with rigid assumptions in the model structure, low hydraulic roughness, and short hillslopes. The proposed model makes some theoretical advancement towards a less scale-dependent way of modeling runoff and erosion on the hillslope-scale, but when calibrated on the watershed-scale, these structural changes bring little predictive gain.

Acknowledgments

The authors would like to thank the staff of the Southwest Watershed Research Center (SWRC) in Tucson, AZ and students from the University of Arizona who helped providing rainfall simulation and other data. We would also like to thank the anonymous reviewers who significantly contributed to the improvement of the first manuscript. The project was funded by the Flemish Agency for the Promotion of Innovation by Science and Technology (IWT) and by a travel grant from the Research Foundation – Flanders (FWO).

References

[1] Joel A, Messing I, Seguel O, Casanova M. Measurement of surface water runoff from plots of two different sizes. Hydrol Process 2002;16:1467–78. http://dx.doi.org/10.1002/hyp.356.
[2] Yair A, Raz-Yassif N. Hydrological processes in a small and catchment: scale effects of rainfall and slope length. Geomorphology 2004;61:155–69. http://dx.doi.org/10.1016/j.geomorph.2003.12.003.
[3] Cerdan O, Le Bissonnais Y, Govers G, Lecomte V, van Oost K, Couturier A, et al. Scale effect on runoff from experimental plots to catchments in agricultural areas in Normandy. J Hydrol 2004;299:4–14. http://dx.doi.org/10.1016/j.jhydrol.2004.02.017.
[4] Lal R. Soil degradative effects of slope length and tillage methods on alfisols in western Nigeria. 1. Runoff, erosion and crop response. Land Degrad Dev 1997;8:201–19.
[5] Le Bissonnais Y. Crusting, runoff and sheet erosion on silty loamy soils at various scales and upscaling from m^2 to small catchments. Soil Tillage Res 1998;46:69–80.
[6] Parsons AJ, Brazier RE, Wainwright J, Powell DM. Scale relationships in hillslope runoff and erosion. Earth Surface Process Landforms 2006;31:1384–93. http://dx.doi.org/10.1002/Esp.1345.
[7] van de Giesen NC, Stomph TJ, de Ridder N. Scale effects of Hortonian overland flow and rainfall–runoff dynamics in a West African catena landscape. Hydrol Process 2000;14:165–75.
[8] Stomph TJ, De Ridder N, Steenhuis TS, van de Giesen NC. Scale effects of Hortonian overland flow and rainfall–runoff dynamics: laboratory validation of a process-based model. Earth Surface Process Landforms 2002;27:847–55. http://dx.doi.org/10.1002/Esp.356.
[9] Wainwright J, Parsons AJ. The effect of temporal variations in rainfall on scale dependency in runoff coefficients. Water Resour Res 2002;38:1267–71. http://dx.doi.org/10.1029/2000wr000188.
[10] Smith RE. Infiltration theory for hydrologic applications. Washington D.C.: American Geophysical Union; 2002.
[11] Woolhiser DA, Goodrich DC. Effect of storm rainfall intensity patterns on surface runoff. J Hydrol 1988;102:335–54.
[12] Wood EF, Sivapalan M, Beven K. Scale effects in infiltration and runoff production. In: Conjunctive water use: proceedings of the Budapest symposium, IAHS1986; 1986.
[13] Corradini C, Morbidelli R, Melone F. On the interaction between infiltration and Hortonian runoff. J Hydrol 1998;204:52–67.
[14] Govindaraju RS, Nahar N, Corradini C, Morbidelli R. Role of run-on for describing field-scale infiltration and overland flow over spatially variable soils. J Hydrol 2004;286:36–51. http://dx.doi.org/10.1016/j.jhydrol.2003.09.011.
[15] Morbidelli R, Corradini C, Govindaraju RS. A field-scale infiltration model accounting for spatial heterogeneity of rainfall and soil saturated hydraulic conductivity. Hydrol Process 2006;20:1465–81. http://dx.doi.org/10.1002/Hyp.5943.
[16] Brooks ES, Boll J, McDaniel PA. A hillslope-scale experiment to measure lateral saturated hydraulic conductivity. Water Resour Res 2004;40:10. http://dx.doi.org/10.1029/2003wr002858. Artn W04208.
[17] Van Nieuwenhuyse BHJ, Antoine M, Wyseure G, Govers G. Pattern-process relationships in surface hydrology: hydrological connectivity expressed in landscape metrics. Hydrol Process 2011;25:3760–73. http://dx.doi.org/10.1002/hyp.8101.
[18] Lyford FP, Qashu HK. Infiltration rates as affected by desert vegetation. Water Resour Res 1969;5:1373–6. http://dx.doi.org/10.1029/WR005i006p01373.
[19] Johnson CW, Gordon ND. Runoff and erosion from rainfall simulator plots on sagebrush rangeland. Trans ASAE 1988;31:421–7.
[20] Bochet E, Poesen J, Rubio JL. Mound development as an interaction of individual plants with soil, water erosion and sedimentation processes on slopes. Earth Surface Process Landforms 2000;25:847–67. http://dx.doi.org/10.1002/1096-9837(200008)25:8<847::aid-esp103>3.0.co;2-q.
[21] Bochet E, Rubio JL, Poesen J. Modified topsoil islands within patchy Mediterranean vegetation in SE Spain. Catena 1999;38:23–44.
[22] Dunne T, Zhang WH, Aubry BF. Effects of rainfall, vegetation, and microtopography on infiltration and runoff. Water Resour Res 1991;27:2271–85.
[23] Cammeraat LH. A review of two strongly contrasting geomorphological systems within the context of scale. Earth Surface Process Landforms 2002;27:1201–22. http://dx.doi.org/10.1002/esp.421.
[24] Bresson LM, Valentin C. Soil surface crust formation – contribution of micromorphology. In: RingroseVoase AJ, Humphreys GS, editors. Soil micromorphology: studies in management and genesis. Amsterdam: Elsevier Science Publ B V; 1994. p. 737–62.
[25] Fox DM, Le Bissonnais Y, Bruand A. The effect of ponding depth on infiltration in a crusted surface depression. Catena 1998;32:87–100.
[26] Langhans C, Govers G, Diels J, Clymans W, Van den Putte A. Dependence of effective hydraulic conductivity on rainfall intensity: loamy agricultural soils. Hydrol Process 2010;24:2257–68.
[27] Langhans C, Govers G, Diels J. Development and parameterization of an infiltration model accounting for water depth and rainfall intensity. Hydrol Process 2013;27:3777–90. http://dx.doi.org/10.1002/hyp.9491.
[28] Langhans C, Govers G, Diels J, Leys A, Clymans W, Putte AVd, et al. Experimental rainfall–runoff data: reconsidering the concept of infiltration capacity. J Hydrol 2011;399:255–62.
[29] Blöschl G, Sivapalan M. Scale issues in hydrological modeling: a review. Hydrol Process 1995;9:251–90. http://dx.doi.org/10.1002/hyp.3360090305.
[30] Stone JJ, Nichols MH, Goodrich DC, Buono J. Long-term runoff database, walnut gulch experimental watershed, Arizona, United States. Water Resour Res 2008;44:1–5. http://dx.doi.org/10.1029/2006wr005733. Artn W05s05.
[31] Osterkamp WR. Geology, soils, and geomorphology of the walnut gulch experimental watershed, Tombstone, Arizona. J Arizona-Nevada Acad Sci 2008;40:136–54.
[32] Paige GB, Stone JJ, Smith JR, Kennedy JR. The walnut gulch rainfall simulator: a computer-controlled variable intensity rainfall simulator. Appl Eng Agric 2004;20:25–31.
[33] Stone JJ, Paige GB, Hawkins RH. Rainfall intensity-dependent infiltration rates on rangeland rainfall simulator plots. Trans ASAE 2008;51:45–53.
[34] Luk SH, Merz W. Use of the salt tracing technique to determine the velocity of overland-flow. Soil Technol 1992;5:289–301.
[35] Green WH, Ampt GA. Studies on soil physics, 1. The flow of air and water through soils. J Agric Sci 1911;4:1–22.
[36] Chow VT, Maidment DR, Mays LW. Applied hydrology. New York: McGraw-Hill; 1988.
[37] Chu ST. Infiltration during an unsteady rain. Water Resour Res 1978;14:461–6.
[38] Emmett WW. Overland flow. In: Kirkby MJ, editor. Hillslope hydrology. New York: Wiley; 1978. p. 145–76.
[39] Hawkins RH. Interpretation of source area variability in rainfall–runoff relations. In: Proceedings of international symposium on rainfall–runoff modeling, Mississippi State Univ., Mississippi State; 1982. p. 303–24.
[40] Yu B, Cakurs U, Rose CW. An assessment of methods for estimating runoff rates at the plot scale. Trans ASAE 1998;41:653–61.
[41] Chen ZQ, Govindaraju RS, Kavvas ML. Spatial averaging of unsaturated flow equations under infiltration conditions over areally heterogeneous fields. 2. Numerical simulations. Water Resour Res 1994;30:535–48.
[42] Polyakov VO, Kimoto A, Nearing MA, Nichols MH. Tracing sediment movement on a semiarid watershed using rare earth elements all rights reserved. no part of this periodical may be reproduced or transmitted in any form or by any means, electronic or mechanical, including photocopying, recording, or any information storage and retrieval system, without permission in writing from

the publisher. Permission for printing and for reprinting the material contained herein has been obtained by the publisher. Soil Sci Soc Am J 2009;73:1559–65. http://dx.doi.org/10.2136/sssaj2008.0378.
[43] Yu B, Rose CW, Ciesiolka CAA, Coughlan KJ, Fentie B. Toward a framework for runoff and soil loss prediction using GUEST technology. Aus J Soil Res 1997;35:1191–212.
[44] Abrahams AD, Parsons AJ. Determining the mean depth of overland flow in field studies of flow hydraulics. Water Resour Res 1990;26:501–3. http://dx.doi.org/10.1029/WR026i003p00501.
[45] Dunkerley D. Estimating the mean speed of laminar overland flow using dye injection-uncertainty on rough surfaces. Earth Surface Process Landforms 2001;26:363–74.
[46] Fox DM, Bryan RB, Price AG. The influence of slope angle on final infiltration rate for interrill conditions. Geoderma 1997;80:181–94.
[47] Risse LM, Nearing MA, Zhang XC. Variability in Green–Ampt effective hydraulic conductivity under fallow conditions. J Hydrol 1995;169:1–24.
[48] Nearing MA, Liu BY, Risse LM, Zhang X. Curve numbers and Green–Ampt effective hydraulic conductivities. J Am Water Resour Assoc 1996;32:125–36. http://dx.doi.org/10.1111/j.1752-1688.1996.tb03440.x.
[49] Burns ISC. Reducing uncertainty in hydrological modeling: a step-wise multi-scale calibration approach [Ms.]. Tucson, AZ: University of Arizona; 2010.
[50] Sharma ML, Gander GA, Hunt CG. Spatial variability of infiltration in a watershed. J Hydrol 1980;45:101–22.
[51] Sharma ML, Barron RJW, Fernie MS. Areal distribution of infiltration parameters and some soil physical properties in lateritic catchments. J Hydrol 1987;94:109–27. http://dx.doi.org/10.1016/0022-1694(87)90035-7.
[52] Smith RE, Goodrich DC. Model for rainfall excess patterns on randomly heterogeneous areas. J Hydrol Eng 2000;5:355–62.